Angle Effects of LIDAR Measurements on a Flat Surface and in High-Velocity Spillway Flows

R. Li
UNSW Sydney

M. Kramer
UNSW Canberra

S. Felder
UNSW Sydney, s.felder@unsw.edu.au

Recommended Citation

Li R., Kramer, M., and Felder, S. (2022). "Angle Effects of LIDAR Measurements on a Flat Surface and in High-Velocity Spillway Flows" in "9th IAHR International Symposium on Hydraulic Structures (9th ISHS)". *Proceedings of the 9th IAHR International Symposium on Hydraulic Structures – 9th ISHS*, 24-27 October 2022, IIT Roorkee, Roorkee, India. Palermo, Ahmad, Crookston, and Erpicum Editors. Utah State University, Logan, Utah, USA, 9 pages (DOI: 10.26077/64f1-4c4b) (ISBN 978-1-958416-07-5).

9th International Symposium on Hydraulic Structures Roorkee, India 24-27 October 2022
ISBN 978-1-958416-07-5 DOI: https://doi.org/10.26077/64f1-4c4b

Angle Effects of LIDAR Measurements on a Flat Surface and in High-velocity Spillway Flows

R. Li[1], K.D. Splinter[1], M. Kramer[2] & S. Felder[1]
[1] *Water Research Laboratory, School of Civil and Environmental Engineering, UNSW Sydney, Australia*
[2]*UNSW Canberra, School of Engineering and Information Technology (SEIT), Canberra, ACT 2610, Australia*
E-mail: s.felder@unsw.edu.au

Abstract: *Measurements in aerated high-velocity spillway flows have been traditionally conducted with point-source instruments. LIDAR is a promising remote sensing technology that may be able to provide more detailed insights into the free-surface properties. So far only one laboratory study has investigated the use of LIDAR technology in air-water flows on a spillway model showing that free-surface data in the aerated part of the flow can be recorded with high spatial and temporal resolution. However, the spillway model, as well as the aerated flow region, were quite short and further research is needed to test the performance of LIDAR technology on a longer spillway. Herein, the present study tested a LIDAR in an 8.6 m long laboratory spillway with strip roughness. To ensure consistency of results along the spillway, the performance of the LIDAR was first assessed without flowing water along a straight wall as well as in the spillway model without water. The results showed that the LIDAR was affected by viewing angle that can be corrected using a scaling factor. The LIDAR was subsequently used to measure the free-surface properties of skimming flows. Comparative results for three different LIDAR measurement positions showed effects on the free-surface elevations and standard deviations linked with the different grazing angle of the LIDAR relative to the free-surface and with the waviness of the free-surface. A potential correction scheme for this is discussed.*

Keywords: *Air-water flows, remote sensing, physical modelling, instrumentation, hydraulic structures, signal processing.*

1. Introduction

High-velocity air-water flows on spillways occur commonly in flow conveyance systems such as spillways and chutes. The flows are non-aerated at the upstream end but become strongly aerated downstream of the inception point of free-surface aeration (Chanson 1996). Highly aerated flows in spillways are characterized by entrapped and entrained air (Killen 1968) where the entrained air penetrates deep into the flow column, while the entrapped air is characterized by free-surface instabilities and waves (Valero and Bung 2016). The air entrainment and entrapment vary strongly in space and time, which makes measurements of the flow depth and other aerated free-surface parameters challenging. Accurate measurements of the free-surface elevations provide important information for the calculation of design parameters such as rate of energy dissipation and flow resistance (Chanson 1996; Wood 1991). In non-aerated flows, pointer gauges and acoustic displacement meters (ADMs) are commonly used for flow depth measurements, while in air-water flows, the most suited instrument are phase-detection intrusive probes (Felder and Chanson 2015, Kramer et al. 2020a). A key limitation of all these instruments is that they provide data at a fixed measurement point and only very limited spatial and temporal information of the flow processes.

Previous studies used ADMs to measure time-varying free-surface features of aerated flows at a single point, revealing free-surface motions with broad frequency spectrum (Zhang et al. 2018). While ADMs appeared to be a suitable instrument for aerated high-velocity flows (Bung 2013; Felder and Chanson 2014), on second look, there is a strong disagreement between characteristic air-water flow elevations measured with a phase-detection probe and the mean elevations measured with ADMs, with variations in void fractions between 50% and 90% (Bung 2013; Felder and Chanson 2014; Kramer and Chanson 2018; Zhang et al. 2018). Several factors may affect the ADM measurements including the ADM type, the size of the ADM beam and the nature of the air-water flows (Li et al. 2021a). In contrast, phase-detection probes are considered very reliable instruments in high-velocity air-water flows on spillways, and have been successfully used for understanding of fundamental flow processes (e.g. Chanson and Toombes 2002; Felder and Chanson 2015) and spillway design (e.g. Felder and Chanson 2016; Hunt et al. 2014; Ohtsu et al. 2004). However, phase-detection intrusive probes only collect information at one location, or if multiple probes are used simultaneously at several locations (Hohermuth et al. 2021). In any case, the calculation of the air-water flow properties, of the characteristic elevations and associated design parameters relies on time and depth averaging.

Other instrumentation may be more promising for the measurement of more spatially- and temporally varying observations of the free-surface. Thorwarth (2008) observed highly non-stationary free-surface motions in pooled

stepped spillways with a video camera, while more recent studies used high-speed cameras to record the air-water properties at the vicinity of the sidewall (Bung and Valero 2016; Zhang et al. 2018). The flow properties next to the sidewall may differ from the channel centerline (Kramer and Chanson 2019), and sidewall measurements are also not a viable option for field measurements. More recently, application of top-view video cameras has been explored in hydraulic jumps (Bung et al. 2020) and spillways (Kramer and Felder 2021) showing promising prospects for the recording of design parameters in the laboratory and in large-scale prototype spillways (Chanson 2022; Kramer and Felder 2021).

Another type of remote sensing instrumentation is LIDAR technology that has been explored across a range of air-water flows, including classical hydraulic jumps (Felder et al. 2021; Li et al. 2021a; Montano et al. 2018), hydraulic jumps in stilling basins (Li et al. 2021b), stepped spillway flows (Kramer et al. 2020b), and a water confluence (Rak et al. 2020). These studies have shown that LIDAR can measure the free-surface of highly aerated flows continuously with high spatial and temporal resolution, allowing a detailed documentation of the dynamic free-surface processes. The application of LIDAR technology in high-velocity flows has been limited to a single investigation in a relatively short, stepped spillway with a short air-water flow region (Kramer et al. 2020b). Kramer et al. (2020b) confirmed the applicability of LIDAR in such flows providing measurements of free-surface elevations, fluctuations, as well as characteristic free-surface time and length scales. A comparison with data recorded with a phase-detection intrusive probe suggested that the LIDAR may be able to predict the void fraction distributions. However, further investigations of LIDAR performance in longer spillways are needed to better understand the LIDAR's ability for potential prototype measurements. Herein, this study applied LIDAR technology in a long spillway model with strip roughness. Following tests of the LIDAR on solid surfaces without flows, this paper presents LIDAR measurements of a skimming flow regime using three different LIDAR positions along the spillway. The results suggested a strong effect of the LIDAR position on the free-surface measurements and a possible correction scheme is discussed.

2. Experiments and Data Processing

New experiments were conducted at the UNSW Water Research Laboratory using a 2D industrial LIDAR (SICK LMS511) with a wavelength of 905 nm and a laser beam width < 20 mm for measurement distances < 10 m (SICK 2015). Simple tests with spacers suggested a smaller beam width of approximately 5 mm in the laboratory (Li et al. 2021a). The same LIDAR was previously used in a range of applications including classical hydraulic jumps (Felder et al. 2021; Montano et al. 2018) and hydraulic jumps in a stilling basin (Li et al. 2021b). For all experiments in the present study, the LIDAR was sampled at 35 Hz with an angular resolution of 0.25º.

In the first experiment, the LIDAR was tested in dry conditions along a concrete flat surface with a length of 12 m (Figure 1). For this experiment, the LIDAR was positioned 1.6 m above the bed. The LIDAR continuously scanned the concrete surface for 60 seconds. The grazing angle between the LIDAR beam and the horizontal surface was indicated by θ (Figure 1).

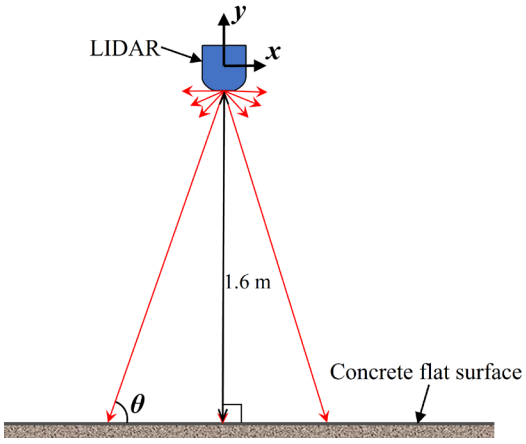

Figure 1. Setup of LIDAR test on long flat surface.

A second set of experiments was conducted in a large-scale spillway model (Figure 2). The spillway had a length of 8.6 m, a width of 0.8 m and a slope of 10.8º. At the spillway's upstream end, a large header tank and a broad-crested

weir with an upstream rounded corner provided steady and smooth inflows. Twenty-four identical wooden strip blocks of 0.07 m width and 0.045m height were installed along the spillway model. The first strip block was positioned 0.24 m from the upstream end to allow smooth transition of flows from the broad-crested weir into the spillway chute. The consistent spacing between blocks was 0.28 m along the spillway (Figure 2c). A flow rate q = 0.288 m^2/s was investigated, which corresponded to a Reynolds number (defined with hydraulic diameter) of 8.4×10^5. The flows resembled skimming flows with a non-aerated flow region at the upstream end, and strongly aerated flows downstream of the inception point of free-surface aeration. The inception point was visually determined and occurred at approximately x = 2.5 m between the 7th and 8th block (Figure 2a). The depth-averaged mean flow aeration was approximately 0.13 at the inception point and approximately 0.2 in the downstream uniform flow region. The free-surface of the flows were parallel to the channel bed skimming over the strip roughness elements while strong fluctuations of the free-surface were consistently observed downstream of the inception point. The flow motions between the strips were characterized by stable recirculation patterns with irregular ejection processes between the cavity and the skimming flows above. For the spillway experiments, the LIDAR was inclined at the same plane as the spillway bed so that $\theta = 90^o$ was perpendicular to the bed (Figure 2b). The LIDAR was positioned at an elevation of 1.5 m above the spillway bed at three longitudinal locations X_{LIDAR} = 2.7, 5.2 and 7.4 m relative to the spillway's upstream end (Figure 2b). These LIDAR positions provided a wide range of grazing angles $10^o \leq \theta \leq 90^o$ along the spillway. For each LIDAR position, the LIDAR continuously measured the dry bed for 5 minutes and measured the flows for 30 minutes along the centerline of the spillway.

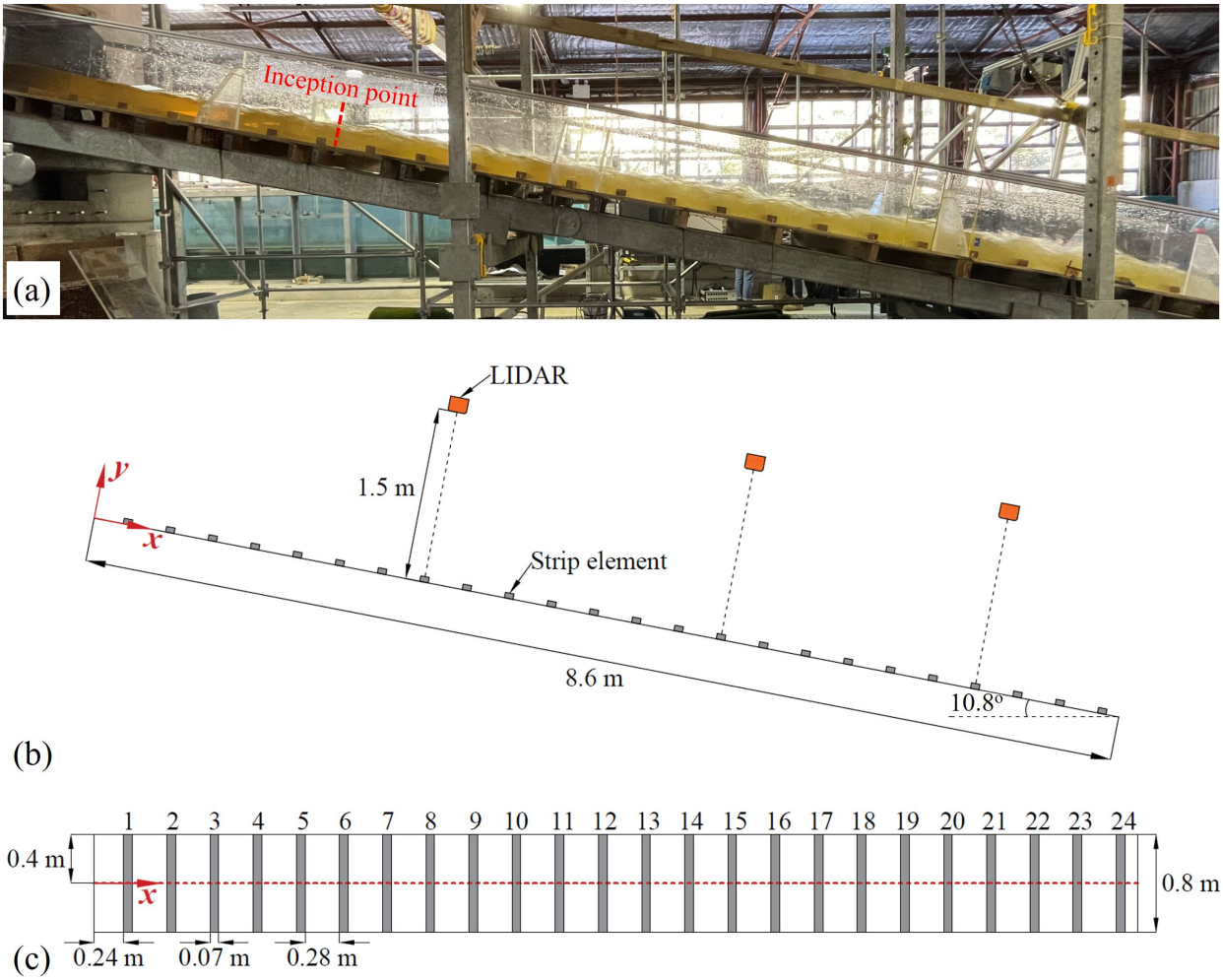

Figure 2. Spillway model in the present study; (a) photo of spillway model and skimming flow patterns for q = 0.288 m^2/s; (b) side-view sketch of the 24 strip roughness elements along the spillway and 3 positions of LIDAR; (c) top-view sketch with the dimensions of the spillway.

For all experiments, the raw signal of distances and angles were recorded using Sopas ET software of SICK. The data processing was conducted in MATLAB following the general procedure presented in Li et al. (2021a). The LIDAR data were first translated into a Cartesian coordinate system. Then all data were interpolated onto a constant x-axis grid based on the average of all recorded frames. Finally, statistical calculations including mean elevations and standard deviations were conducted using the interpolated data. Note that for the spillway experiments, meaningless signals below the channel bed were replaced with NaNs, and no signal filtering was applied in the present study.

3. Results (1): LIDAR Tests in Dry Conditions

Figure 3 shows the mean profiles of the flat concrete surface measured by the LIDAR and corresponding grazing angles. Note that the figure was not scaled to clearly show the measurement distortion on a long flat surface. It appeared that the LIDAR slightly overestimated the surface elevation with increasing distances and decreasing grazing angles resulting in a slight distortion curvature. This effect was also observed in previous studies using LIDAR to measure long straight surfaces (Martins 2017; Streicher et al. 2013). Martins (2017) indicated that this could be due to the energy distribution over the elliptical footprint. According to Katzenbeisser (2003), this distortion might be linked with the scaling of viewing angle and can be corrected using a scaling factor. Different correction factors were tested for the present case and a factor of -0.0027 performed the best for the present LIDAR to adjust the distortion. This means that the grazing angle θ was adjusted as:

$$\theta = 0.9973 \times \theta_{raw} + 0.243 \quad (1)$$

where θ_{raw} is the grazing angle recorded by the LIDAR before correction.

After the distortion correction with Eq. (1), the uncertainty of mean LIDAR elevations on a flat surface was less than 10 mm for a measurement range up to 12 m with $10^o \leq \theta \leq 90^o$ (Figure 3a). Since Eq. (1) linearly scaled the grazing angles, the standard deviations y' of LIDAR measurements using raw and corrected LIDAR signals were similar and are shown in Figure 3b. The standard deviations were lower than 10 mm for measurement distances up to 12 m with the sampling time of 60 s (> 2100 data points). For grazing angles larger than 40°, y' was approximately 4 mm, while y' increased for lower grazing angles. This can be linked with longer measurement distances and larger elliptical footprint of the LIDAR signal (SICK 2015; Soudarisssanane et al. 2011). In the present study, all LIDAR measurements on the large-scale spillway were corrected using Eq. (1) to eliminate the distortion due to angle at large distances. Note that the distortion effect was only observed in the long spillway and not in the much shorter air-water flow phenomena (e.g., hydraulic jumps) investigated in previous studies (e.g. Li et al. 2021b; Montano et al. 2018).

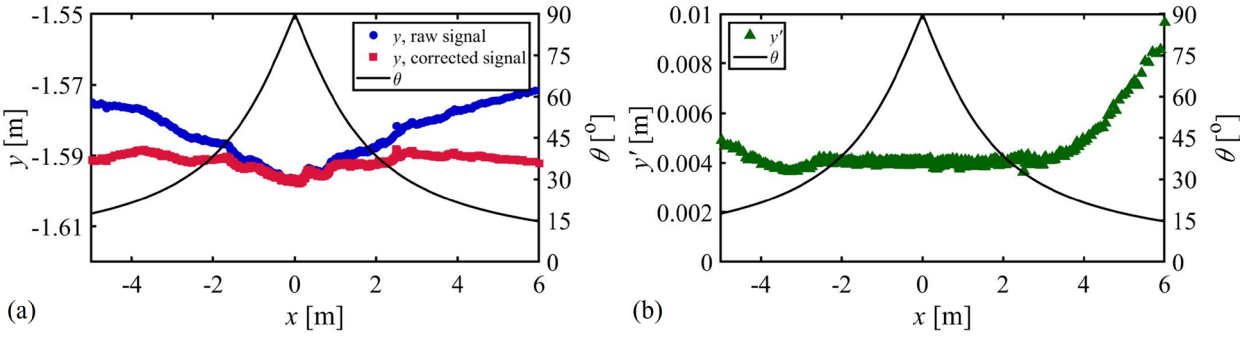

Figure 3. LIDAR measurements on flat straight concrete surface: (a) surface profile measured with the LIDAR; (b) standard deviation of the LIDAR signal.

Figure 4 shows the mean bed profiles measured with the LIDAR positioned at X_{LIDAR} = 5.2 m before and after the correction using the angle scaling factor described above (Eq. (1)). The bed profile after angle scaling compared well with the measured bed profile with an average difference of 3 mm for all data points along the spillway. The standard deviation of the bed measurements was less than 6 mm along the spillway. In contrast to the flat bed tests presented above, the strip roughness had an additional source of error due to signal blocking induced by low grazing angles. This was most apparent in the cavity between strip elements at locations further away from the LIDAR (i.e., smaller θ at

the upstream and downstream end) where the elevated strip blocked the signal from resolving the vertical edge and subsequent cavity. This is visible in Figure 4, particularly for $x < 2.4$ m, where less data points along the bed are resolved compared to closer to the LIDAR position.

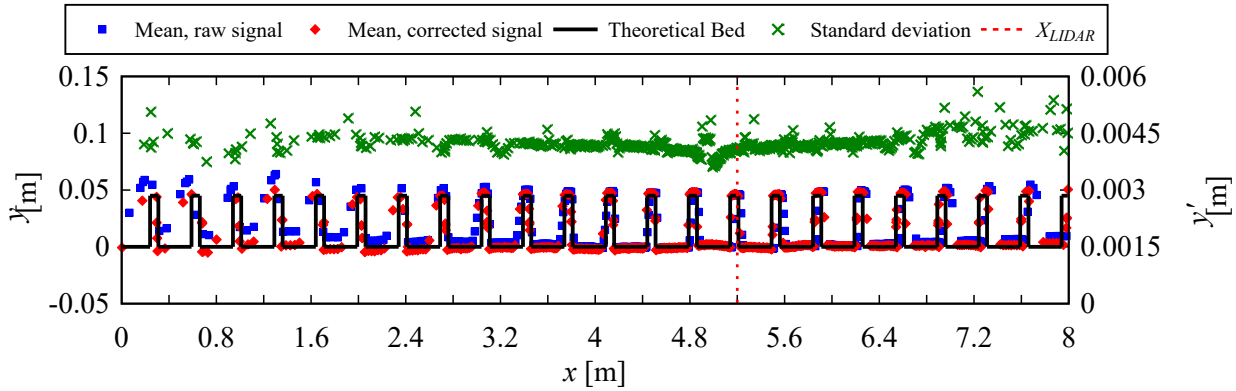

Figure 4. Comparison between the spillway bed measured with the LIDAR before and after distortion correction; standard deviation of the LIDAR measurements (X_{LIDAR} = 5.2 m, Y_{LIDAR} = 1.5 m).

4. Results (2): Free-surface Elevations in Skimming Flows along Spillway with Strip Roughness

Now that a correction method has been established for the LIDAR data to account for angle effects, measurements of free-surface flows are presented. Figure 5 shows typical instantaneous free-surface profiles from the upstream end to the aerated region recorded by the LIDAR for the three LIDAR positions. The measurements with high temporal and spatial resolution enhanced the visualization of the fast free-surface fluctuations and advection of free-surface waves along the spillway. Notably, additional videos generated using raw LIDAR signals (not shown here) suggested that the LIDAR was able to continuously track the free-surface waves propagating along the spillway.

As shown in Figure 5, there is clear differences in the instantaneous free-surface profiles measured for the three different LIDAR positions. This was linked with both the flow aeration levels and the LIDAR positioning effects. The LIDAR was not able to consistently record the free-surface in the flows with low flow aeration since LIDAR signals tended to penetrate into the flow (Allis et al. 2011; Montano et al. 2018; Rak et al. 2017). This resulted in the very low LIDAR elevations close to the bed at locations upstream of and close to the inception point and was most noticeable for the LIDAR positioned near the inception point (X_{LIDAR} = 2.7 m). In the downstream aerated region, the instantaneous free-surface profiles were consistent with visual observations showing strong free-surface fluctuations. However, it can be observed that the LIDAR position also influenced the overall signal with stronger free-surface fluctuations recorded near the LIDAR for all three positions. As such, an upstream positioned LIDAR tended to measure higher free-surface elevations in the downstream aerated region (Figure 5a), while the LIDAR positioned at the downstream end recorded lower signals in the water column (Figure 5c). This was linked with the effect of grazing angles, since LIDAR signals with small grazing angles might be blocked by the extensive water splashes and free-surface perturbations in the air-water flow and is further discussed in Section 5.

Figure 6 shows the mean free-surface elevations d recorded by the LIDAR for the three LIDAR positions. The free-surface standard deviations d' recorded by the LIDAR were added as whiskers (Figure 6). The LIDAR was not able to record the free-surface profile in the non-aerated region upstream of the inception point ($x < 2.5$ m), which was expected due to LIDAR signal penetration into the flow. In the region just downstream of the inception point ($2.5 < x < 5$ m), measurements with a LIDAR position close to the measurement locations (X_{LIDAR} = 2.7 m) were still affected by the low flow aeration leading to low mean free-surface profiles (Figure 6a). In the downstream strongly aerated region ($x > 5$ m), differences up to 30% were observed between the mean free-surface elevations recorded with different LIDAR positions (Figure 6a). The free-surface standard deviations d' recorded with different LIDAR positions showed a relative difference up to 50% in the aerated flow (Figure 6b). As noted above, the large differences in free-surface properties recorded with different LIDAR positions are due to different grazing angles of the LIDAR signal and the wavy nature of the free-surface. These effects and a potential method to interpret LIDAR measurements in aerated spillway flows are further discussed in Section 5.

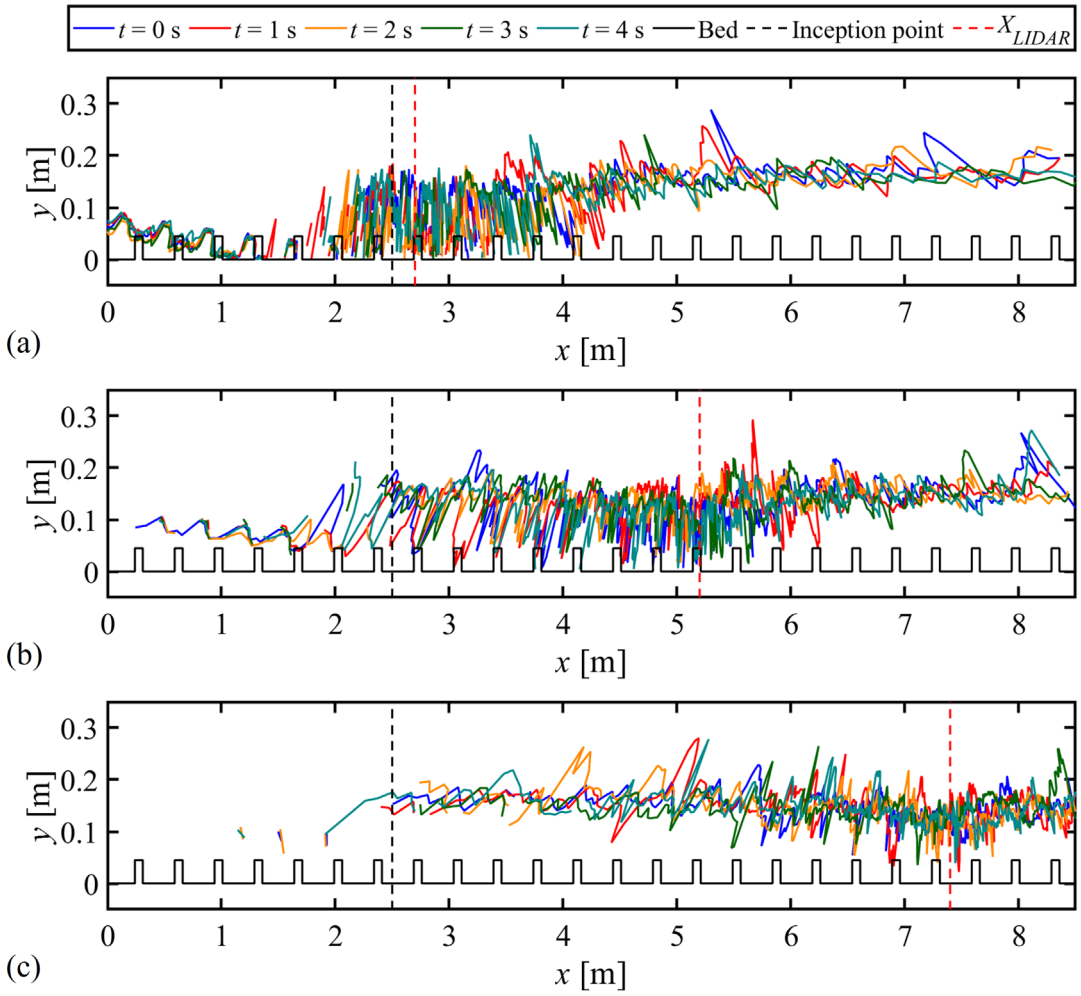

Figure 5. Instantaneous free-surface profiles using corrected LIDAR data for 3 LIDAR positions at 5 consecutive seconds in the skimming flows on the spillway: (a) X_{LIDAR} = 2.7 m; (b) X_{LIDAR} = 5.2 m; (c) X_{LIDAR} = 7.4 m.

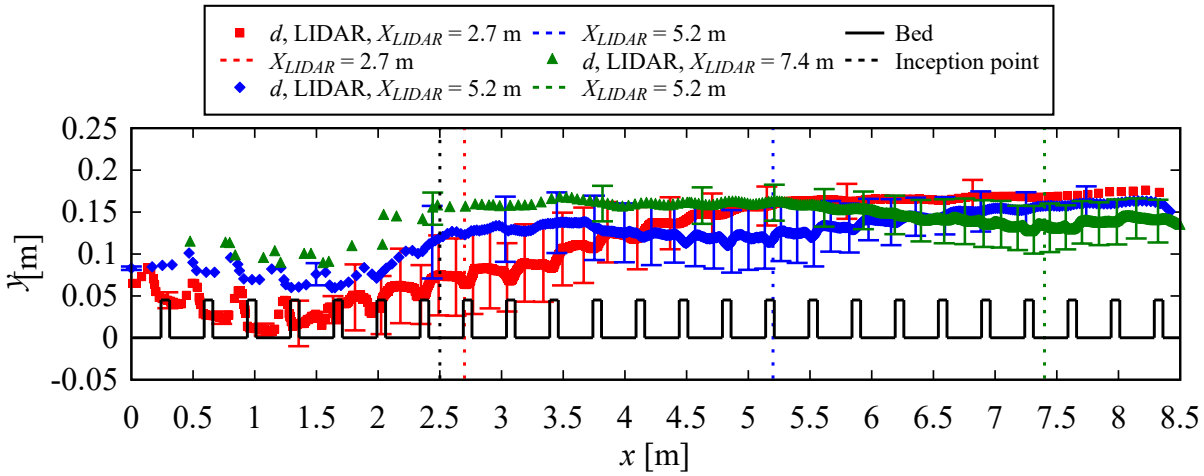

Figure 6. Comparison between the free-surface elevations recorded with the LIDAR for three LIDAR positions; whiskers indicate the standard deviations in free-surface elevations.

5. Discussion

Differences in air-water flow free-surface properties recorded with different LIDAR positions were previously observed in hydraulic jumps (Li et al. 2021a). Li et al. (2021a) suggested LIDAR positions upstream of the jump toe to avoid signal blocking due to free-surface waves and water ejections in the jump roller. These issues have also been noted by researchers studying breaking waves and bores in the surf zone (Blenkinsopp et al. 2010; Martins et al. 2016). In the present study, LIDAR tests in the dry bed conditions on the spillway with strip roughness showed that small grazing angles resulted in signal blocking by strip roughness elements at certain locations. Similarly, the large differences in free-surface properties measured with different LIDAR positions in the high-velocity air-water flows were linked with the angle effects and the nature of the free-surface. While some of these angle effects are due to internal properties of the LIDAR and can be corrected for using Eq. (1), other factors are a function of the aerated flows themselves. Figure 7 presents a sketch to further describe the angle effects in the aerated skimming flows. When grazing angles are close to 90°, i.e. the LIDAR is directly above the point of interest, there is a higher probability of the signal penetrating deeper into the air-water flows. In the inception region with little flow aeration, a LIDAR positioned close to the measurement point tended to penetrate deeper into the flow before hitting a bubble to reflect off, while a LIDAR positioned far from the point penetrated less into the flow before hitting a bubble (Figure 7b). This was also due to internal properties of the LIDAR where longer measurement distances caused larger and elliptical footprints of the LIDAR beam, as well as lower signal strength (SICK 2015; Soudarissanane et al. 2011) resulting in less penetration through the surface in the non-aerated region. In the downstream aerated region with strong free-surface perturbations, an oblique LIDAR signal with small grazing angle was not able to record the troughs of free-surface waves or the entrained bubbles, since the LIDAR signal was blocked by the peaks of the free-surface waves and water splashes. This effect resulted in elevated free-surface profile measured by an oblique LIDAR with small grazing angles (Figure 7c).

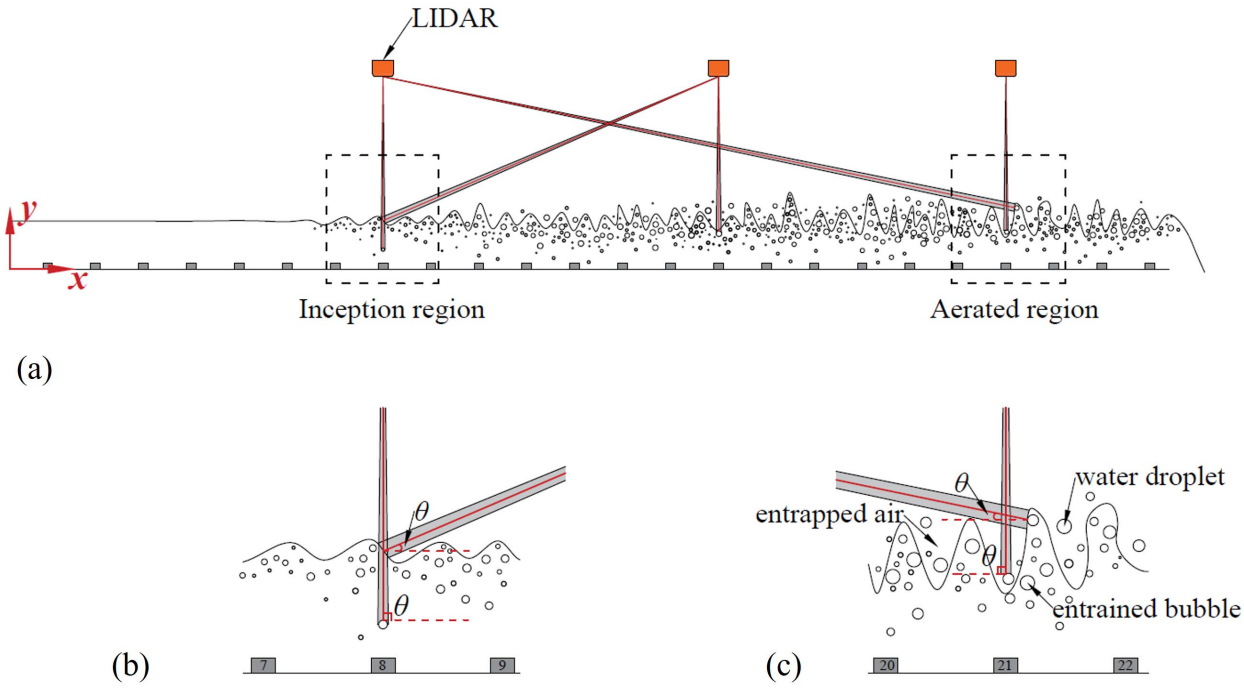

Figure 7. Sketch of the angle effect on the free-surface measurements in skimming flows: (a) angle effect along the spillway; (b) angle effect in the inception region with low flow aeration; (c) angle effect in the aerated flow region.

Conceptually, the link between entrained bubbles and LIDAR have been presented by several authors. Montano (2019) and Li et al. (2021b) showed that the mean LIDAR elevations in aerated hydraulic jumps were close to the elevations with maximum bubble count rate. Additionally, Kramer et al. (2020b) showed that the LIDAR signal distribution was comparable to the distribution of bubble count rate in the downstream aerated region and proposed that the LIDAR signal was able to measure the bubbles in aerated flows. Preliminary analysis of the present spillway experiments also observed similar distributions of LIDAR signal and bubble count rate irrespective of the LIDAR position (not shown

here). The comparison between LIDAR measurements and bubble count rate pointed out a promising direction for the correction of the angle effects presented in this manuscript. With this correction method it is believed that all signals can be aligned irrespective of the LIDAR position, enabling the use of LIDAR measurements to understand internal air-water flow properties. Current research is therefore combining measurements of LIDAR with intrusive air-water flow conductivity probes.

6. Conclusion

The present study tested the performance of LIDAR technology on a long flat concrete surface as well as in high-velocity skimming flow in a spillway with strip roughness. The mean elevations of the flat concrete surface measured with the LIDAR showed slight distortion due to scaling of viewing angles. A correction equation was proposed to correct the distortion of all LIDAR measurements with low grazing angles. In the high-velocity spillway flow, the LIDAR was not able to measure the free-surface in the non-aerated region, while the LIDAR captured distinct free-surface waves propagating along the spillway and strong free-surface fluctuations in the aerated region. The LIDAR measurements with different LIDAR positions showed differences up to 30% in mean free-surface elevations and differences up to 50% in standard deviations in the aerated flow. These differences were linked with different grazing angles and the nature of the aerated flows with free-surface waves and perturbations. Comparison between LIDAR signal distribution and bubble count rate distribution may provide opportunities to correct LIDAR signals for the prediction of internal air-water flow properties and is a topic of current research.

7. ACKNOWLEDGMENTS

The authors thank Rob Jenkins (Water Research Laboratory, UNSW Sydney) for his technical help.

8. REFERENCES

Allis, M.J., Peirson, W.L., and Banner, M.L. (2011). "Application of LiDAR as a measurement tool for waves." *Proc., International Offshore and Polar Engineering Conference*, Hawaii, USA, 8, 373–379.

Blenkinsopp, C.E., Mole, M.A., Turner, I.L., and Peirson, W.L. (2010). "Measurements of the time-varying free-surface profile across the swash zone obtained using an industrial LIDAR." *Coast. Eng*., 57(11–12), 1059–1065.

Bung, D.B. (2013). "Non-intrusive detection of air-water surface roughness in self-aerated chute flows." *J. Hydraul. Res*., 51(3), 322–329.

Bung, D.B., Crookston, B.M., and Valero, D. (2020). "Turbulent free-surface monitoring with an RGB-D sensor: the hydraulic jump case." *J. Hydraul. Res*., 59(5), 779–790.

Bung, D.B., and Valero, D. (2016). "Optical flow estimation in aerated flows." *J. Hydraul. Res*., 54(5), 575–580.

Chanson, H. (1996). Air bubble entrainment in free-surface turbulent shear flows, Academic Press Inc, San Diego, California, USA.

Chanson, H. (2022). "On Air Entrapment Onset and Surface Velocity in High-Speed Turbulent Prototype Flows." *Flow Meas. Instrum*., 83, Paper 102122.

Chanson, H., and Toombes, L. (2002). "Air–water flows down stepped chutes: turbulence and flow structure observations." *Int. J. Multiph. Flow*, 28(11), 1737–1761.

Felder, S., and Chanson, H. (2014). "Air-water flows and free-surface profiles on a non-uniform stepped chute." *J. Hydraul. Res*., 52(2), 253–263.

Felder, S., and Chanson, H. (2015). "Phase-detection probe measurements in high-velocity free-surface flows including a discussion of key sampling parameters." *Exp. Therm. Fluid Sci*., 61, 66–78.

Felder, S., and Chanson, H. (2016). "Simple Design Criterion for Residual Energy on Embankment Dam Stepped Spillways." *J. Hydraul. Eng*., 142(4), 04015062.

Felder, S., Montano, L., Cui, H., Peirson, W., and Kramer, M. (2021). "Effect of inflow conditions on the free-surface properties of hydraulic jumps." *J. Hydraul. Res*., 59(6), 1004–1017.

Hohermuth, B., Boes, R.M., and Felder, S. (2021). "High-velocity air-water flow measurements in a prototype tunnel chute – scaling of void fraction and interfacial velocity." *J. Hydraul. Eng*., 147(11), 04021044.

Hunt, S.L., Kadavy, K.C., and Hanson, G.J. (2014). "Simplistic Design Methods for Moderate-Sloped Stepped Chutes." *J. Hydraul. Eng*., 140(12), 04014062.

Katzenbeisser, R. (2003). "On the calibration of lidar sensors." *Proc., ISPRS 3-D Workshop Reconstruction from Airborne Laser-Scanner and InSAR Data*, Dresden, Germany, 59–64.

Killen, J. M. 1968. "The Surface Characteristics of Self Aerated Flow in Steep Channels." Ph.D Thesis, University of Minnesota, Minneapolis, USA.

Kramer, M., and Chanson, H. (2018). "Free-surface instabilities in high-velocity air-water flows down stepped chutes." *Proc., 7th International Symposium on Hydraulic Structures*, Aachen, Germany.

Kramer, M., and Chanson, H. (2019). "Optical flow estimations in aerated spillway flows: Filtering and discussion on sampling parameters." *Exp. Therm. Fluid Sci*., 103, 318–328.

Kramer, M., Hohermuth, B., Valero, B., and Felder, S. (2020a). "Best practices for velocity estimations in highly aerated flows with dual-tip phase-detection probes." *International Journal of Multiphase Flow*, 126, 103228.

Kramer, M., Chanson, H., and Felder, S. (2020b). "Can we improve the non-intrusive characterization of high-velocity air–water flows? Application of LIDAR technology to stepped spillways." *J. Hydraul. Res*., 58(2), 350–362.

Kramer, M., and Felder, S. (2021). "Remote sensing of aerated flows at large dams: proof of concept." *Remote Sens*., 13(14), 2836.

Li, R., Splinter, K.D., and Felder, S. (2021a). "Aligning free surface properties in time-varying hydraulic jumps." *Exp. Therm. Fluid Sci*., 126, 110392.

Li, R., Splinter, K.D., and Felder, S. (2021b). "LIDAR Scanning as an Advanced Technology in Physical Hydraulic Modelling: The Stilling Basin Example." *Remote Sens*., 13(18), 3599.

Martins, K. (2017). "Wave transformation in the surf-zone." Ph.D Thesis, University of Bath, UK.

Martins, K., Blenkinsopp, C.E., and Zang, J. (2016). "Monitoring Individual Wave Characteristics in the Inner Surf with a 2-Dimensional Laser Scanner (LiDAR)." *J. Sensors*, 2016, 1–11.

Montano, L. (2019). "An experimental study of free surface dynamics and internal motions in fully aerated hydraulic jumps." Ph.D. thesis, School of Civil and Environmental Engineering, University of New South Wales, Sydney, Australia.

Montano, L., Li, R., and Felder, S. (2018). "Continuous measurements of time-varying free-surface profiles in aerated hydraulic jumps with a LIDAR." *Exp. Therm. Fluid Sci*., 93, 379–397.

Ohtsu, I., Yasuda, Y., and Takahashi, M. (2004). "Flow Characteristics of Skimming Flows in Stepped Channels." *J. Hydraul. Eng*., 130(9), 860–869.

Rak, G., Hočevar, M., and Steinman, F. (2017). "Measuring water surface topography using laser scanning." *Flow Meas. Instrum*., 56, 35–44.

Rak, G., Steinman, F., Hočevar, M., Dular, M., Jezeršek, M., and Pavlovčič, U. (2020). "Laser ranging measurements of turbulent water surfaces." *Eur. J. Mech. B/Fluids*, 81, 165–172.

SICK. (2015). LMS5xx Laser Measurement Sensors: Operating Instructions. Germany.

Soudarissanane, S., Lindenbergh, R., Menenti, M., and Teunissen, P. (2011). "Scanning geometry: Influencing factor on the quality of terrestrial laser scanning points." *ISPRS J. Photogramm. Remote Sens*., 66(4), 389–399.

Streicher, M., Hofland, B., and Lindenbergh, R.C. (2013). "Laser Ranging For Monitoring Water Waves In The New Deltares Delta Flume." *Proc., ISPRS Workshop Laser Scanning*, Antalya, Turkey, 271–276.

Thorwarth, J. (2008). "Hydraulisches Verhalten der Treppengerinne mit eingetieften Stufen – Selbstinduzierte Abflussinstationaritäten und Energiedissipation. (Hydraulics of Pooled Stepped Spillways – Self-induced Unsteady Flow and Energy Dissipation.)." Ph.D Thesis, University of Aachen, Germany (in German).

Valero, D., and Bung, D.B. (2016). "Development of the interfacial air layer in the non-aerated region of high-velocity spillway flows. Instabilities growth, entrapped air and influence on the self-aeration onset." *Int. J. Multiph. Flow*, 84, 66–74.

Wood, I.R. (1991). "Free surface air entrainment on spillways." Air Entrainment in Free-surface Flows, I.R. Wood, ed., IAHR, Hydraulic Structures Design Manual 4, Hydraulic Design Considerations, A.A. Balkema, Rotterdam, the Netherlands, 55–84.

Zhang, G., Valero, D., Bung, D.B., and Chanson, H. (2018). "On the estimation of free-surface turbulence using ultrasonic sensors." *Flow Meas. Instrum*., 60, 171–184.